Induced Strain Actuation of Isotropic and Anisotropic Plates

E. F. Crawley* and K. B. Lazarus†
Massachusetts Institute of Technology, Cambridge, Massachusetts 01239

The development and experimental verification of the induced strain actuation of plate components of an intelligent structure is presented. Equations relating the actuation strains, created by induced strain actuators, to the strains induced in the actuator/substrate system are derived for isotropic and anisotropic plates. Plate strain energy relations are also developed. Several exact solutions are found for simple actuator/substrate systems, and a general procedure for solving the strain energy equations with a Rayleigh-Ritz technique is formulated. Approximate Ritz solutions lead to both an understanding of the system design parameters and to detailed models of cantilever plate systems. Simple test articles were used to verify the accuracy of the basic induced strain actuator/substrate system models, and cantilever plate test articles were built and tested to verify the ability of the models to predict the strains induced in systems with extensive stiffness coupling and complicated boundary conditions.

Introduction

INDUCED strain actuation is the process by which actuation strain in some elements of the structure induces deformation of the overall structure. Actuation strain is the general term applied to strain components other than those caused by stress. Natural mechanisms that cause actuation strains include thermal expansion,[1] piezoelectricity,[2] electrostriction,[3] magnetostriction,[4] material phase change,[5] or moisture absorption.[6]

When the actuation strain mechanism is easily regulated, as in the case of piezoelectricity, induced strain actuation can be used to control the deformations of intelligent structures, i.e., structures with distributed actuator and sensor systems. For example, it can be used to control the extension, bending, and twisting of plate-like structures without producing rigid body forces and torques or inertial loads. It has advantages over other types of actuation because the actuators are easily integrated with load bearing structures by surface bonding or embedding[2] and do not significantly alter the passive static or dynamic stiffness characteristics of the structures.[7] Used in conjunction with tailored anisotropic composite materials, control of specific static deformations or modes can be greatly enhanced.[9]

Isotropic and anisotropic plates with distributed induced strain actuators could be used for the pointing of precision instruments,[8] optical system mirror or reflector shape control,[10] and the active acoustical control of structure borne noise.[11] An example of a specific application of induced strain actuation would be the bonding of induced strain actuators to a load bearing structure of an aeroelastic lifting surface.[8] The actuation could be used to alter the shape of the lifting surface, thereby changing the lift on the vehicle. Thus, aerodynamic control is effected without the use of articulated structures and linkages necessary for conventional aerodynamic control surfaces. Aeroelastic applications of this induced strain actuator system include the quasistatic control of the camber and twist of aerodynamic surfaces, and dynamic control of the deformations for gust alleviation and flutter suppression.

Received June 22, 1989; revision received Dec. 27, 1989; accepted for publication Jan. 7, 1990.

*Associate Professor, Space Engineering Research Center, Department of Aeronautics and Astronautics. Associate Fellow AIAA.

†Graduate Research Assistant, Space Engineering Research Center, Department of Aeronautics and Astronautics. Member AIAA.

To date, detailed models of induced strain actuator systems are limited. Models of strain actuators coupled with simple beams[2,12,13,14] and plates,[7,8] and models of isolated piezoelectric plates[15,16] currently exist. There is a need for a more general model of the induced strain actuation of plates with various boundary conditions and externally applied loads. Such models should treat isotropic and anisotropic plates that are entirely or partially covered with piezoelectric actuators in various orientations. The models should incorporate surface bonded and embedded actuators and be accurate for both static and dynamic applications. It is the objective of this work to develop and verify such a modeling capability.

A model of induced strain actuator systems, which combines both the actuators and the substrates into one integrated structure, will be developed. This model, referred to as the "consistent plate model," considers the induced strain actuators to be plies of a laminated plate. The consistent plate model relations lead to direct formulation of the plate equations of elasticity and strain energy equations. A limited number of exact solutions to the equations of elasticity are presented, as is a Ritz approach to finding approximate solutions for more general geometries. Representative Ritz solutions are derived that show the options for exploiting the combination of anisotropic material properties and induced strain actuation to bring about bending and twisting of plates. The models and solutions developed were verified experimentally. Simple sandwich and more representative cantilever plate articles were built and the induced strains and deformations measured. The results demonstrate the validity of the models developed, and the effectiveness of using induced strain actuation for shape control of elastic structures.

Analytical Modeling

Derivation of the Consistent Plate Model

The consistent plate actuation model treats both the actuators and the structural plate substrates as plies of an integrated laminated plate. In the following analysis, no assumptions with regard to the actuator placement, actuator symmetry, or the component isotropy will be made. Any number of arbitrarily positioned and oriented surface bonded or embedded actuators, combined with substrates of arbitrary stiffness properties, can be modeled. The only assumptions made will be those normal to thin and classical laminated plate theory.[17]

The term "consistent plate model" comes from the assumption of consistent deformations in the actuators and substrates. The strain distribution is assumed to result from a linear combination of in-plane extensional (constant strain through the thickness) and bending (linearly varying through the thickness) displacements. This assumed strain distribution,

in contrast to several other possibilities, has been found to most accurately represent the actual behavior, even in the case of discrete surface bonded actuators.[18] The strain in the system will therefore depend on the midplane strain ϵ^o and the curvature κ.[17]

$$\epsilon = \epsilon^o + z\kappa \qquad \epsilon^o = \begin{Bmatrix} \epsilon_x^o \\ \epsilon_y^o \\ \gamma_{xy}^o \end{Bmatrix} = \begin{Bmatrix} \dfrac{\partial u}{\partial x} \\ \dfrac{\partial v}{\partial y} \\ \dfrac{\partial u}{\partial y} + \dfrac{\partial v}{\partial x} \end{Bmatrix}$$

$$\kappa = \begin{Bmatrix} \kappa_{xx} \\ \kappa_{yy} \\ \kappa_{xy} \end{Bmatrix} = \begin{Bmatrix} -\dfrac{\partial^2 w}{\partial x^2} \\ -\dfrac{\partial^2 w}{\partial y^2} \\ -2\dfrac{\partial^2 w}{\partial x \partial y} \end{Bmatrix} \tag{1}$$

The constitutive relation for a homogeneous plate, or for any ply of a laminated plate is

$$\sigma = \mathbf{Q}(\epsilon - \Lambda) = \mathbf{Q}\epsilon - \mathbf{Q}\Lambda \tag{2}$$

where the stress vector and the actuation strain vector are

$$\sigma = [\sigma_x \ \sigma_y \ \tau_{xy}]^T \qquad \Lambda = [\Lambda_x \ \Lambda_y \ \Lambda_{xy}]^T \tag{3}$$

The matrix $\mathbf{Q}$ is the transformed reduced stiffness of the plate or one of its plies in the plate axis system.[1] The second term $\mathbf{Q}\Lambda$ in Eq. (2) represents the equivalent stress created as a result of the actuation strains. The actuation strain vector Λ contains in-plane normal and shear strain components, and enters into the elasticity equations in the same manner as does thermal strain. Actuation strain is the strain that physically causes induced strains to be produced, and can be due to thermal expansion, piezoelectricity, electrostriction, etc.

The consistent plate load deformation relations can be found by substituting the assumed deformation [Eq. (1)] into the stress-strain equation [Eq. (2)] and integrating through the thickness t of the plate

$$\begin{bmatrix} \bar{\mathbf{N}} \\ \bar{\mathbf{M}} \end{bmatrix} = \begin{bmatrix} \mathbf{A} & \mathbf{B} \\ \mathbf{B} & \mathbf{D} \end{bmatrix} \begin{bmatrix} \epsilon^o \\ \kappa \end{bmatrix} - \begin{bmatrix} \mathbf{N}_\Lambda \\ \mathbf{M}_\Lambda \end{bmatrix} \tag{4}$$

where the conventional mechanical force and moment resultants are

$$\bar{\mathbf{N}} = \int_t \sigma \, dz \qquad \bar{\mathbf{M}} = \int_t \sigma z \, dz \tag{5}$$

The matrixes $\mathbf{A}$, $\mathbf{B}$, and $\mathbf{D}$ are the usual extensional, coupling and bending stiffnesses of the plate. The equivalent actuator forces $\mathbf{N}_\Lambda$ and moments $\mathbf{M}_\Lambda$ per unit length are

$$\mathbf{N}_\Lambda = \int_t \mathbf{Q}\Lambda \, dz \qquad \mathbf{M}_\Lambda = \int_t \mathbf{Q}\Lambda z \, dz \tag{6}$$

Care must be taken in performing the necessary integrations to obtain the correct stiffness and actuator forcing terms. Both actuator and substrate plies contribute to the stiffness matrixes $\mathbf{A}$, $\mathbf{B}$, and $\mathbf{D}$, whereas only actuator plies contribute to the actuator forcing vectors $\mathbf{N}_\Lambda$ and $\mathbf{M}_\Lambda$, which are dependent on the mode of actuation (prescribed actuation strains). Extensional actuation is effected by prescribing actuation strains that are symmetric about the neutral axis, while bending actuation results when the actuation strains in the actuators above the neutral axis are prescribed to be in opposition (180 deg out of phase) to those below the neutral axis.

Equation 4 relates the resultant total strains and curvatures found in the actuator/substrate system to the actuation strains, external loads, and stiffness properties of the system in a general and compact form. The presence of numerous coupling terms shows that it is possible to create a variety of deformations (e.g., bending or twisting) using several different actuation modes (e.g., extension or bending). Thus, by careful selection of the laminate ply orientations, an actuator/substrate system can be designed to effect control for a variety of applications. In addition, various couplings may be introduced by the boundary conditions, as would be the case for a swept cantilever wing.

Difficulty in solving the induced strain plate equations exactly indicates the necessity to derive approximate methods based on the strain energy relations. The consistent plate model can be used to formulate the strain energy relations for a laminated plate. The total potential energy stored in a plate undergoing induced strain actuation is

$$U = \frac{1}{2}\int_A \int \{\epsilon^{oT} \ \kappa^T\} \begin{bmatrix} \mathbf{A} & \mathbf{B} \\ \mathbf{B} & \mathbf{D} \end{bmatrix} \begin{Bmatrix} \epsilon^o \\ \kappa \end{Bmatrix} d(A) - \int_A \int [\mathbf{N}_\Lambda \ \mathbf{M}_\Lambda] \begin{Bmatrix} \epsilon^o \\ \kappa \end{Bmatrix} d(A) \tag{7}$$

This strain energy equation, along with a Ritz approximate solution method, will be used to solve for the approximate strains and curvatures induced in plate actuator systems.

Exact Solutions

Several exact solutions to the consistent plate model equations [Eq. (4)] are now presented for free-free-free-free plates, with no externally applied loads. In these solutions, it will be assumed that the in-plane actuation strains are isotropic, and there is no actuation shear strain:

$$\Lambda = [\Lambda \ \Lambda \ 0]^T \tag{8}$$

Explicit solutions for the induced strains and curvatures can be found for isotropic systems by assuming the Poisson ratio of the actuator and substrate are identical, and inserting the appropriate isotropic extensional A and bending D stiffness matrixes (B = 0) into Eq. (4). Assuming the actuator placement is symmetric about the midplane, the strain and curvature relations uncouple and are

$$\begin{bmatrix} \epsilon \\ \kappa \end{bmatrix} = \begin{bmatrix} \dfrac{\alpha_1}{\alpha_1 + \psi} \begin{bmatrix} 1 & 0 & 0 \\ 0 & 1 & 0 \\ 0 & 0 & 1 \end{bmatrix} \Lambda & [0] \\ [0] & \dfrac{2}{t_s}\left[\dfrac{1}{T} + 1\right] \dfrac{\alpha_2}{\alpha_2 K + \psi} \begin{bmatrix} 1 & 0 & 0 \\ 0 & 1 & 0 \\ 0 & 0 & 1 \end{bmatrix} \Lambda \end{bmatrix}$$

$$T = \frac{t_s}{t_a} \qquad K = \frac{4}{3}\left(\frac{1}{T}\right)^2 + 2\left(\frac{1}{T}\right) + 1 \qquad \psi = \frac{E_s t_s}{E_a t_a} \tag{9}$$

where the subscripts s and a refer to the substrate and actuator, respectively. The effectiveness of the induced strain actuation, i.e., the magnitude of the resultant strains and curvatures induced, depends on the actuation strain Λ, relative stiffness

ratio ψ, thickness ratio T, and geometric constant α.[2] The geometric constant is a function of the mode of actuation and the system configuration. For a system of two actuators bonded symmetrically to a substrate, $\alpha_1 = 2$ for extensional actuation and $\alpha_2 = 6$ for bending actuation. It is clear that as the plate stiffness decreases, so does the relative stiffness parameter, and the effectiveness of the strain transfer from actuation strain to induced strain is increased.

It is not as simple to find exact solutions for systems with anisotropic substrates, for which the governing equations are highly coupled. Some insight into the behavior of anisotropic systems can be found by examining an actuator system with an orthotropic substrate. Assuming that the substrate has a Poisson ratio ν_{xy} equal to the Poisson ratio of the actuator ν, and no extension/bending coupling ($\mathbf{B} = 0$), the strains induced due to extensional actuation can be found by substituting the orthotropic substrate properties into Eq. (4):

$$\epsilon_x = \left[\frac{\alpha}{\alpha+\psi}\right]\Lambda$$

$$\epsilon_y = \left[\frac{\alpha\left\{\nu\left[\frac{1}{\gamma}\left(\alpha+\psi\right)-\left(\frac{\alpha}{\gamma}+\psi\right)\right]+\left(\frac{1}{\gamma}-\nu^2\right)(\alpha+\psi)\right\}}{(\alpha+\psi)\left(\frac{\alpha}{\gamma}+\psi\right)-\nu^2(\alpha+\psi)^2}\right]\Lambda$$

$$\gamma_{xy} = 0 \tag{10}$$

where γ is the ratio of the transverse to longitudinal elastic moduli E_y/E_x of the substrate, and the relative stiffness ratio ψ is now given by $E_x t_s/E_a t_a$. It can be seen that anisotropic strains will be induced in the actuator/substrate system. The degree of anisotropy of the induced strains will depend on the ratio of the plate stiffness in the longitudinal and transverse directions γ. Also, because the actuation strains were assumed to be isotropic and it was assumed that the substrate had no extension/shear coupling, no shear strain will be induced in the substrate.

For substrate components constructed from a general composite laminate, Eq. (4) indicates that a fully populated 6×6 element stiffness matrix must be inverted. It can be seen that shear strain will be induced in systems with extension/shear coupling (e.g., A_{16}), twist curvature will be induced in systems with extension/twist coupling (e.g., B_{16}) when actuated in extension, and twist curvature will be induced in systems with bending/twist coupling (e.g., D_{16}) when actuated in bending. However, no further insight is found by attempting to invert the stiffness matrix.

Ritz Formulation for Approximate Solutions

Closed form solutions cannot be found for the majority of induced strain actuator configurations. For systems with more complex geometry, boundary conditions, and externally applied loads, approximate solution methods must be utilized. A Ritz solution is presented that gives approximate solutions, yet still allows insight into the physics of induced strain actuation. A matrix notation is adopted that leads to compact representations of the governing equations.

Solutions are desired for extensional and bending actuation of systems with extensive stiffness couplings. Therefore, it is essential that the in-plane as well as the out-of-plane deformations are adequately represented. The plate systems will be considered to have both in-plane and out-of-plane displacements, and a displacement vector defined as

$$\mathbf{u} = \{u\ v\ w\}^T \tag{11}$$

where u and v are the longitudinal x and transverse y in-plane displacements, respectively, and w is the out-of-plane displacement.

Using the above representation for the displacements [Eq. (11)], the strains and curvatures can be expressed as

$$\begin{Bmatrix} \epsilon^o \\ \kappa \end{Bmatrix} = [\mathfrak{D}]\{\mathbf{u}\} \tag{12}$$

where $\mathfrak{D}$ is a derivative operator matrix

$$\mathfrak{D} = \begin{bmatrix} \frac{\partial}{\partial x} & 0 & \frac{\partial}{\partial y} & 0 & 0 & 0 \\ 0 & \frac{\partial}{\partial y} & \frac{\partial}{\partial x} & 0 & 0 & 0 \\ 0 & 0 & 0 & -\frac{\partial^2}{\partial x^2} & -\frac{\partial^2}{\partial y^2} & -2\frac{\partial^2}{\partial x \partial y} \end{bmatrix} \tag{13}$$

and the strains and curvatures are defined in Eq. (1).

The assumed shape functions chosen will depend on the geometry, boundary conditions, and forcing of each individual system, but in general the displacements can be written as

$$\{\mathbf{u}\} = [\mathbf{H}]\mathbf{q}$$

$$H = \begin{bmatrix} [\phi_{u_1}, \phi_{u_2}, \ldots, \phi_{u_m}] & [0] & [0] \\ [0] & [\phi_{v_1}, \phi_{v_2}, \ldots, \phi_{v_n}] & [0] \\ [0] & [0] & [\phi_{w_1}, \phi_{w_2}, \ldots, \phi_{w_p}] \end{bmatrix} \tag{14}$$

where ϕ_{u_i}, ϕ_{v_j}, and ϕ_{w_k} are, respectively, the longitudinal in-plane, transverse in-plane, and transverse out-of-plane assumed shape functions, which are functions of x and y. The vector $\mathbf{q}$ is the generalized coordinate vector, and the matrix $\mathbf{H}$ is a 3 by r (total number of assumed functions $r = m + n + p$) dimensional matrix of the assumed shape functions.

An expression for the strain energy in terms of the assumed shape functions can be found by substitution of Eqs. (12) and (14) into the strain energy equation [Eq. (7)]

$$U = \tfrac{1}{2}\mathbf{q}^T\mathbf{K}\mathbf{q} - \mathbf{Q}_\Lambda\mathbf{q}$$

$$\mathbf{K} = \int_A \int (D\mathbf{H})^T \begin{bmatrix} \mathbf{A} & \mathbf{B} \\ \mathbf{B} & \mathbf{D} \end{bmatrix} (D\mathbf{H})\, \mathrm{d}(A)$$

$$\mathbf{Q}_\Lambda = \int_A \int (D\mathbf{H})^T \begin{Bmatrix} \mathbf{N}_\Lambda \\ \mathbf{M}_\Lambda \end{Bmatrix} \mathrm{d}(A) \tag{15}$$

In the energy expression above, $\mathbf{K}$ is the usual r by r stiffness matrix, and $\mathbf{Q}_\Lambda$ can be described as the r by 1 actuation strain forcing vector, since it represents the forces acting on the assumed shape functions that develop from the actuation strains.

The static or dynamic response can be calculated by combining the strain energy expression with appropriate energy principles, such as Lagrange's equations. The resulting strains and curvatures can be found directly from Eqs. (12) and (14).

Design Parameters for Coupled Plates

Insight can be gained and important design parameters revealed by obtaining explicit Ritz solutions for particular assumed deformations. A design question to be addressed, for example, is as follows: Because common induced strain actuators do not produce shear, how can plate twist be effected? The minimum representative set of assumed functions needed

to address this issue includes those associated with longitudinal extension, bending, and twisting, so that bending/twisting and extension/twisting coupling can be examined. Using only these shape functions is equivalent to assuming that the transverse extension, transverse bending, and the net in-plane shear are zero.

The three shape functions associated with extension (shape 1), bending (shape 5), and twisting (shape 6) are shown in Table 1. Inserting these modes into the Ritz model, the stiffness matrix **K** and the actuation strain forcing vector $\mathbf{Q}_\Lambda$ become

$$\mathbf{K} = \begin{bmatrix} A_{11} & -2\frac{1}{L}B_{11} & -2\frac{1}{C}B_{16} \\ -2\frac{1}{L}B_{11} & 4\frac{1}{L^2}D_{11} & 4\frac{1}{CL}D_{16} \\ -2\frac{1}{C}B_{16} & 4\frac{1}{CL}D_{16} & 4\frac{1}{C^2}D_{66} \end{bmatrix} \quad \mathbf{Q}_\Lambda = \begin{bmatrix} (N_\Lambda)_x L \\ 2(M_\Lambda)_x \\ 0 \end{bmatrix} \tag{16}$$

where L is the longitudinal x and C is the transverse y plate dimension. The rows of the forcing vector correspond to extensional, bending, and twist deformation. The third or twist forcing term in $\mathbf{Q}_\Lambda$, which is proportional to the actuation shear strain, is zero.

Twist deformation can be obtained by making use of bending actuation and bending/twist coupling D_{16}. Setting the extension/bending B_{11} and extension/twist B_{16} coupling terms to zero in the stiffness matrix [Eq. (16)], and solving for the static twist curvature by substituting the calculated twist amplitude into Eqs. (12) and (14) yields

$$\kappa_{xy} = -\frac{1}{2}\left[\frac{D_{16}}{D_{11}D_{66} - D_{16}^2}\right](M_\Lambda)_x \tag{17}$$

The twist curvature depends on the ratio of the coupling stiffness D_{16} to the bending stiffness D_{11} and the torsional stiffness D_{66}. It is convenient to define a bending/twist coupling parameter ψ_D as

$$\psi_D = \frac{D_{16}}{\sqrt{D_{11}D_{66}}} \tag{18}$$

This parameter can be used to compare the relative amount of bending/twist coupling in various systems for the purpose of design.

Table 1 Cantilever plate assumed shape functions for static deformations

Assumed shape	Associated deformation	Shape function
In-plane displacements		
1	Longitudinal extension	$\frac{x}{L}$
2	Longitudinal shear	$\frac{x}{L}\frac{y}{C}$
3	Transverse extension	$\frac{y}{C}$
4	Transverse shear	$\frac{x}{L}$
Out-of-plane displacements		
5	Longitudinal bending	$\left(\frac{x}{L}\right)^2$
6	Twist	$\frac{x}{L}\frac{y}{C}$
7	Transverse bending	$\frac{x}{L}\left(\frac{y}{C}\right)^2$

Alternatively, twist curvature can be induced from actuation in the extensional mode by using the extension/twist coupling B_{16} term. Setting the extension/bending B_{11} and the bending/twist D_{16} stiffness terms to zero, and solving for the static twist curvature as above, gives

$$\kappa_{xy} = \frac{1}{2}\left[\frac{B_{16}}{A_{11}D_{66} - B_{16}^2}\right](N_\Lambda)_x \tag{19}$$

In this mode of actuation, the twist depends on the extension/twist stiffness B_{16}, the extensional stiffness A_{11}, and the torsional stiffness D_{66}. The relationship can be characterized by an extension/twist coupling parameter ψ_B

$$\psi_B = \frac{B_{16}}{\sqrt{A_{11}D_{66}}} \tag{20}$$

The extension/twist coupling parameter serves as an indicator of the twist magnitude induced by extensional actuation, and plays an important role in the design of systems with externally applied in-plane loads.

Designing an induced strain actuator system that makes use of the extension/twist coupling parameter ψ_B is a potentially desirable alternative to designing one that takes advantage of the bending/twist coupling parameter ψ_D. It is often desirable to exploit bending/twist coupling to tailor the passive deformations of plates due to out-of-plane loading. An obvious example would be the problem of using induced strain actuation to control an aeroelastic surface that has already been passively tailored using bending/twist coupling.

Experimental Verification

Sandwich Experiments

For the purposes of experimental verification, two sets of specimens were constructed and tested. Piezoelectric Products G-1195 piezoceramics, with a thickness of 0.25 mm, were used as the induced strain actuator in all specimens. The first set of test articles was made of a piezoceramic actuator symmetrically sandwiched between two identical structural plates ($\alpha = \frac{1}{2}$). The sandwich specimens were tested in extension, with free boundary conditions and no external loads applied. These articles were designed and tested so that the analytic models could easily be verified.

Four 5.1 cm square substrate/actuator/substrate sandwiches were constructed, three with aluminum and one with Hercules AS4/3501 Graphite/Epoxy substrates (Table 2). Because the graphite/epoxy substrates were constructed from two uni-directional plies, the fiber volume of the plates was reduced to 39%, reducing the plate engineering constants to $E_L = 95.8$ GPa and $E_T = 6.7$ GPa. The moduli of the aluminum and piezoceramic were assumed to be 70 and 63 GPa, respectively. The plates were bonded together using room temperature cure Ecobond 45 Epoxy, and the bond-layer thickness was less than 0.01 mm.

For an idealized model of piezoceramic actuation, the in-plane actuation strain is isotropic, and proportional to the mechanical/electrical coupling coefficient d_{31} and applied field $\mathcal{E}_3$, as discussed in the Appendix. Each sandwich specimen was tested up to a maximum applied field of 551 V/mm, which is equivalent to 67% of the G-1195 coercive field (the field at which the piezoceramic is depoled). Because of the hysteretic behavior of piezoceramics, a procedure was followed to allow consistent comparisons of results. Before taking data, the applied field was cycled from maximum positive field (against the poling direction) to maximum negative field, and then returned to zero. Then the field was increased against the poling direction and extensional strains were recorded. The strains were defined using the one-sided definition given in Eq. (A2). This procedure was consistent with that followed in obtaining the data used to calculate the mechanical/electrical coupling coefficient of the piezoceramic.

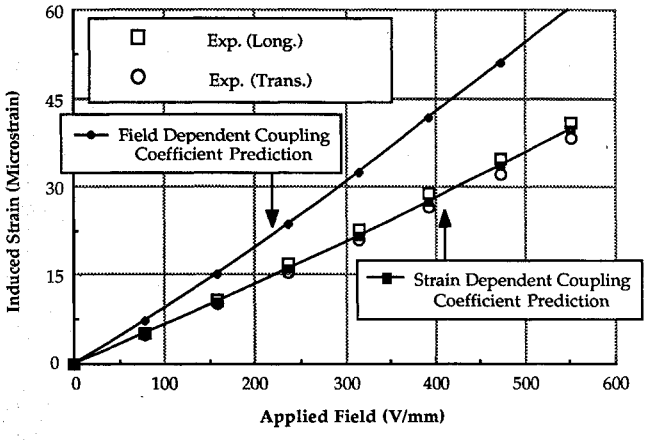

Fig. 1 Induced strain vs field for the aluminum sandwich with 0.32 mm thick substrates. Plots of exact solutions using a strain dependent coupling coefficient and a field dependent coupling coefficient, along with experimental results, are shown.

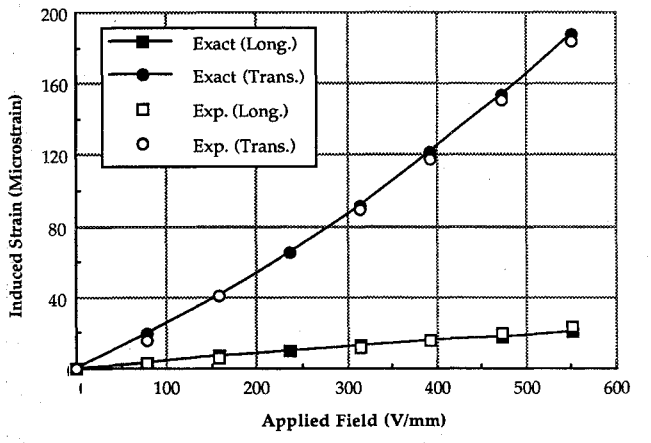

Fig. 2 Induced strain vs field for the graphite/epoxy sandwich. Plotted are the theoretical and experimental results in the longitudinal and transverse dimensions.

The experimental results and analytical predictions for the 0.32 mm aluminum and the graphite/epoxy sandwich are displayed in Figs. 1 and 2, respectively, and the results, at the maximum applied field, of all four sandwich articles tested are shown in Table 2. By comparing the magnitude of the measured strains with those predicted using Eqs. (9) and (10), it can be seen that the model accurately predicts the induced strains in the sandwiches. For the relatively high field reported in Table 2, the average prediction error is 7.5%, with a maximum error of 15.8%.

The data from the aluminum specimen tests reported in Table 2 show how the induced strain varies with the relative stiffness ratio ψ. The strain increased as the relative stiffness ratio decreased, as predicted by Eq. (9). Figure 1 clearly shows the existence of the limited degree of orthotropy associated with piezoceramic actuators, but that the effect on the induced strain is minimal. The maximum variation of the induced strains, between the longitudinal and transverse direction, in the aluminum sandwiches was found to be only 7.4%. By comparison, the induced strains in the graphite/epoxy sandwich shown in Fig. 2 illustrate the significant effect of orthotropy in the substrate on the induced strains.

The analytical predictions for the test articles make use of a mechanical/electrical coupling coefficient (d_{31}), which is dependent on the induced strain, as summarized in the Appendix. Across the four test articles, the induced strains were found to vary significantly, due to the relative stiffness ratios, the range of applied fields, and the effect of orthotropy in the graphite/epoxy substrate. This wide variation in induced strain led to large differences in the predicted coupling coefficients. The coupling coefficients reported in Table 2 for the three aluminum articles showed an increase of 0.8%, 3.5%, and 7.1% over the nominal zero induced strain value of 254 pm/V. The good agreement betwen the analysis and experiment verifies the dependence of the coupling coefficient on the induced strain. Further, induced strains based on an applied field dependent coupling parameter do not correlate with the experiments, as seen in Fig. 1. Finally, the coupling coefficients in the graphite/epoxy sandwich exceed the nominal value by 1.6% and 39.4% in the longitudinal and the transverse directions. The correlation here verifies that the mechanical/electrical coupling coefficients (d_{31} and d_{32}) in orthogonal directions with differing elastic constraints can be determined independently.

Table 2 Sandwich specimen results at 551 V/mm

	AL	AL	AL	G/E
t_s, mm	0.84	0.51	0.32	0.41
ψ	3.67	2.22	1.39	2.23
Induced strain ϵ_L(longitudinal $\mu\epsilon$)				
Experiment	14.6	28.1	38.1	23.2
Exact solution	16.9	26.6	39.7	20.4
Induced strain ϵ_T(transverse $\mu\epsilon$)				
Experiment	15.1	28.2	40.9	183.2
Exact solution	16.9	26.6	39.7	187.0
Strain ratio (ϵ_L/ϵ_T)				
Experiment	1.03	1.00	1.07	7.90
Exact solution	1.00	1.00	1.00	9.17
Predicted coupling coefficients $d(pm/V)$				
Long. d_{31}	256	263	272	258
Trans. d_{32}	256	263	272	354
Predicted actuation strains $\Lambda(\mu\epsilon)$				
Long. Λx	141	145	150	142
Trans. Λy	141	145	150	195

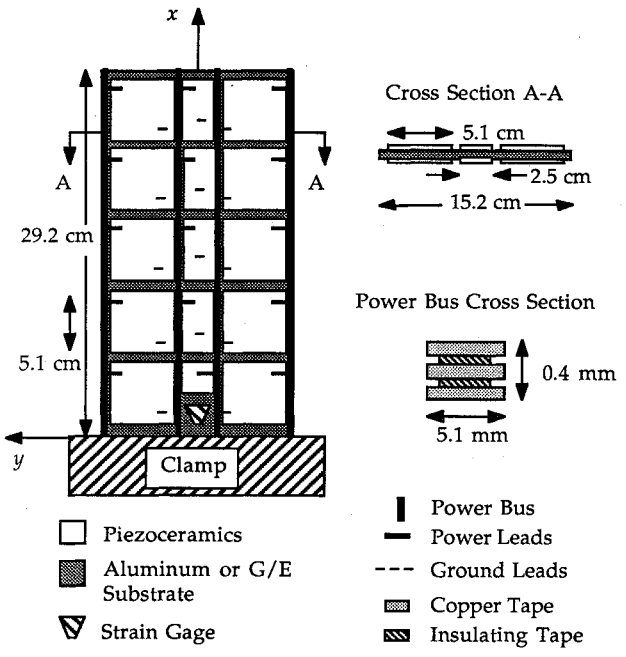

Fig. 3 Cantilever plate symmetric actuator/substrate system. Figure shows coordinate axis, geometry, and placement of the induced strain actuators.

Cantilever Plate Experiments

Cantilever actuator/plate systems, consisting of a single structural plate with piezoceramic actuators symmetrically bonded to both surfaces, were also constructed and tested. These test articles, which were more representative of practical induced strain actuator/substrate systems, were used to verify the ability to predict the actual deflection shapes and applied

field/deformation relations of systems with more complex geometries and boundary conditions, and to verify the Ritz model.

These test articles had 15 actuators bonded to each surface of each plate, as shown in Fig. 3. The actuators covered 71% of the plate surface, and power was applied to the actuators by the power busses and leads indicated in the figure, which were arranged so that either extensional or bending actuation could be effected. Of the four plate systems constructed, one was made of aluminum and the remaining three were constructed from Hercules AS4/3501 Graphite/Epoxy, with $E_L = 143$, $E_T = 9.7$, $\nu_{LT} = 0.3$, and $G_{LT} = 6.0$. The aluminum plate served as an isotropic bench mark specimen, and each graphite/epoxy plate was designed to exploit a specific directional stiffness and produce certain desired deformations. A $[0/\pm 45]_s$ plate was designed for increased transverse bending, a $[+30_2/0]_s$ plate was designed to produce twist through bending/twist coupling ($\psi_D = 0.31$), and a $[+45_3/-45_3]$ plate was designed to take advantage of extension/twist coupling to produce twist ($\psi_B = 0.36$). To prevent any prewarping due to thermal effects, the upper and lower portions of the $[+45_3/-45_3]$ plate were cured separately and then bonded together with a room temperature cure epoxy. All plates were actuated in bending, except for the $[+45_3/-45_3]$ plate, which was actuated in extension.

The deflection data was obtained using three noncontacting proximity sensors and 33 plate mounted targets. Three targets were placed along the transverse y direction at eleven longitudinal x stations. Three targets were used in the transverse direction in order to resolve out-of-plane deflections due to longitudinal bending, twist, and transverse bending. The positions of these measurements were at the outer transverse edges (referred to as M_1 and M_3) and at the center of the plate (M_2). The same experimental procedure used for the sandwich articles was used to record the deflections of the cantilever plate specimens. One row of data was recorded at a time and resolved into three nondimensional displacements

$$W_1 = M_2/C \qquad W_2 = [(M_3 - M_1)/C]$$

$$W_3 = \frac{M_2 - (M_3 + M_1)/2}{C} \tag{21}$$

where C denotes the width, in the transverse direction, of the plate. Physically, W_1 is the nondimensional longitudinal bending, W_2 is the twist in radians, and W_3 is the fractional transverse camber.

The Ritz model in Eq. (15) along with the piezoceramic actuation strain relation in Eq. (A6) was used to analytically predict the deflections. The assumed shape functions utilized in the Ritz solution are listed in Table 1. The clamped boundary condition has been enforced in the in-plane modes to the extent that displacements are constrained at the fixed edge. The longitudinal component of the shear strain (shape 2) can be approximated as a linear function in x, such that the u displacement goes to zero at the clamped edge. The transverse y component of the normal strain (shape 3) requires a higher order function to properly capture the rapid decrease in normal strain near the fixed edge, but to first order this deformation shape can be approximated by a uniform strain in y. The displacement boundary condition will be rigorously enforced for the out-of-plane deflections, while the slope boundary condition will be enforced for longitudinal bending, but not for twist or transverse bending.[19] The twist curvature κ_{xy} (shape 6) and transverse curvature κ_{yy} (shape 7) should be higher order functions of x because of the effects of the fixed edge. However, these shape functions can be approximated by a linear function in x, such that displacements are zero at the clamped edge and maximum at the free end.

The predicted and measured deformations are displayed in Figs. 4, 5, 6, and 7 in the form of nondimensional displacements as a function of longitudinal position. For the plates actuated in bending, it can be seen that the longitudinal deformations approximately follow a quadratic function, which is closely approximated by the Ritz assumed shape function. Also, the twist deformation appears to be nearly linear over the length of the plate as assumed in the Ritz model, except near the clamped edge. This is due to the zero slope conditions enforced by the cantilever boundary. In contrast the transverse bending displacements appear to be a more complicated function than the assumed linear distribution. The transverse bending deflection starts at zero at the fixed end and climbs

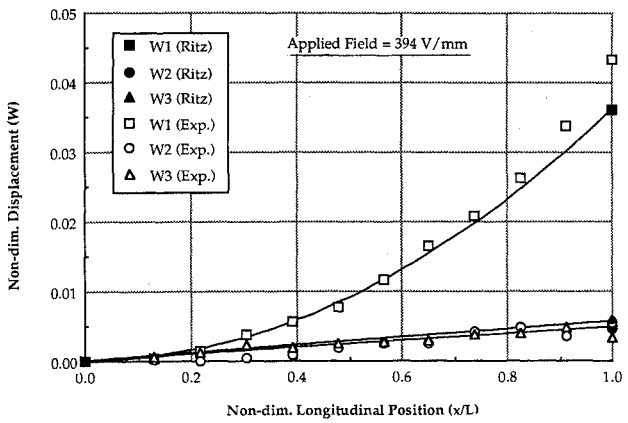

Fig. 5 Graphite/epoxy $[0 \pm 45]_s$ plate theoretical and experimental static deflection shape. Figure shows the nondimensional out-of-plane displacements for bending actuation at an applied field of 394 V/mm.

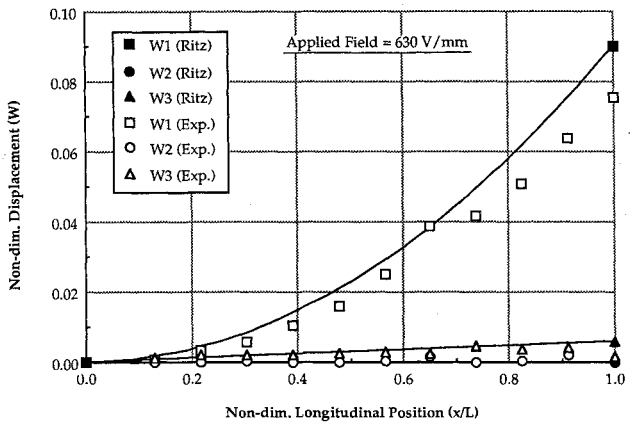

Fig. 4 Aluminum plate theoretical and experimental static deflection shape. Figure shows the nondimensional out-of-plate displacements for bending actuation at an applied field of 630 V/mm.

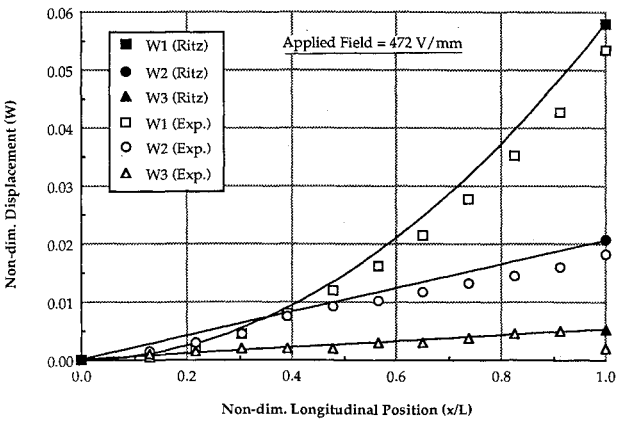

Fig. 6 Graphite/epoxy $[+30_2/0]_s$ plate theoretical and experimental static deflection shape. Figure shows the nondimensional out-of-plane displacements for bending actuation at an applied field of 472 V/mm.

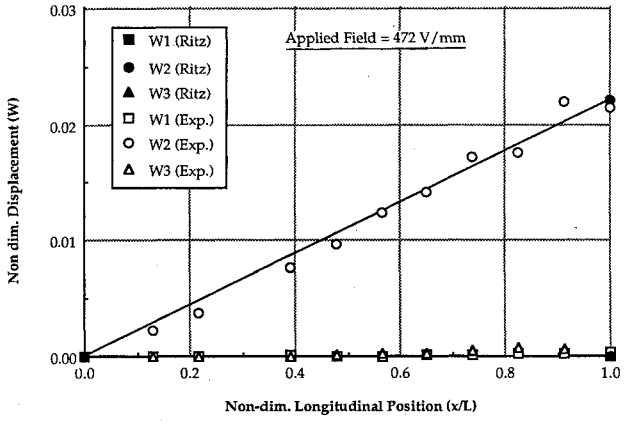

Fig. 7 Graphite/expoxy $[+45_3/-45_3]$ plate theoretical and experimental static deflection shape. Figure shows the nondimensional out-of-plane displacements for extensional actuation at an applied field 472 V/mm.

Table 3 Cantilever plate specimen results at 315 V/mm

	AL	G/E	G/E	G/E
Ply sequence	—	$[0/\pm 45]_s$	$[30_2/0]_s$	$[45_3/-45_3]$
t_s, mm	0.79	0.83	0.83	0.83
ψ	4.90	9.36	9.36	9.36
Longitudinal bending W_1				
Experiment	0.036	0.034	0.035	—
Ritz	0.038	0.028	0.036	—
Twist deformation W_2				
Experiment	—	0.0038	0.0106	0.0140
Ritz	—	0.0036	0.0128	0.0141
Transverse bending W_3				
Experiment	0.0021	0.0028	0.0026	—
Ritz	0.0020	0.0032	0.0028	—

approximately linearly, but drops off sharply at the free longitudinal end. Note that the transverse deformations were found to be significantly smaller than the longitudinal deformations. On average, the transverse deformations were only 8.9% of the longitudinal deformations. For the $[+45_3/-45_3]$ plate actuated in extension, no longitudinal or transverse bending deformations were observed and the twist deformations were found to be nearly linear.

Results of the deflections vs applied field test are summarized in Table 3 for representative sections of each plate. The tip was chosen for comparison of the longitudinal bending and twist deformations. The section chosen for comparison of transverse bending was the three-fourths point along the longitudinal dimension, due to the consistent decrease in transverse bending at the tip. The deflections are presented at the reference applied field of 315 V/mm, since above this field deflections greater than 10 times the plate thickness were observed. The deflections in terms of the plate thickness can be obtained by multiplying the reported values by the inverse of the thickness ratio C/t_s which was 192 for the aluminum plates and 182 for the graphite/epoxy plates. Deflections greater than this could cause nonlinear plate stiffening terms to become significant and the Ritz predictions to deviate from the actual deflections. At this applied field the Ritz solution overpredicted the longitudinal bending deflection by only 5.6% for the aluminum plate as shown in Table 3.

The $[0/\pm 45]_s$ graphite/epoxy plate was designed for increased transverse bending, possessing a longitudinal bending stiffness 28.2% higher than the aluminum plate and a transverse bending stiffness 16.9% less. As expected, Table 3 shows that the magnitude of the deflections recorded for this plate were less in longitudinal bending, by 5.6%, and greater in transverse bending, by 33.3%, than the aluminum plate. Good agreement between experimental results and theoretical predictions was also found for the bending/twist coupled $[+30_2/0]_s$ plate. At the reference applied field the Ritz solution predicted deflections which were 2.8% and 20.7% higher than the experimentally measured values for longitudinal bending and twist deformation, respectively. It was observed that the $[+45_3/-45_3]$ graphite/epoxy plate produced twist deformations which were 32% larger than the deformations produced by the bending/twist coupled $[+30_2/0]_s$ plate, even though the torsional stiffness of the $[+45_3/-45_3]$ plate was 11% higher. The twist deformations predicted by the Ritz solution for this plate were virtually identical to the experimentally measured values.

Conclusions

One of the essential capabilities for the development of controlled intelligent structures is the accurate, a priori, prediction of deformations due to distributed actuators, such as induced strain actuators. A modeling capability for the induced strain actuation of isotropic and anisotropic plates has been developed and verified experimentally. Equations relating the actuation strains created in the actuators to the strains induced in the actuator/substrate system were derived, and the plate strain energy relations were developed using the consistent plate model.

Exact solutions to the equations derived showed that the resulting induced strains and curvatures produced through strain actuation are dependent on the actuation strains Λ, the relative stiffness ratio ψ, and the geometry of the system α. It was also shown that the curvatures induced were dependent on the plate thickness ratio T, and orthotropic strains can be produced by incorporating isotropic induced strain actuators with orthotropic substrates. A Rayleigh-Ritz approximate solution, using the plate strain energy equations, was developed for analyzing systems with complicated stiffness couplings, arbitrary boundary conditions, and external loads.

It was shown that specific deformations can be created in plate actuator/substrate systems by taking advantage of stiffness coupling in the substrate. Specifically, twist deformations can be obtained, using isotropic actuators, through bending actuation and bending/twist stiffness coupling (e.g., D_{16}), or extensional actuation and extension/twist stiffness coupling (e.g., B_{16}). Either method could be used if the other is needed for passive tailoring. Additionally, a simplified Ritz analysis was performed to reveal the important design parameters for achieving such deformations. These parameters were found to be the bending/twist coupling parameter ψ_D and the extension/twist coupling parameter ψ_B.

The models developed were verified through experimentation. A set of simple test articles showed the validity and accuracy of the basic induced strain actuation models. These tests also verified the dependence of the piezoceramic mechanical/electrical coupling coefficient on induced strain. A set of cantilever plate test articles showed the ability of the models to predict the induced strains for more representative systems, and that relatively large deflections can be obtained through induced strain actuation. Substantial agreement between the experimentally measured and analytically predicted deformations was found, verifying the models developed, and demonstrating that induced strain actuation is an effective means of controlling plate deformations.

Appendix: Piezoceramic Properties

Piezoceramics are sources of induced strain that can easily be incorporated into actuator/substrate systems through surface bonding or embedding techniques. Ideally, they can be commanded to create in-plane actuation strains Λ, which are proportional to the mechanical/electrical coupling coefficient d_{31} of the ceramic and applied electric field $\mathcal{E}_3$:

$$\Lambda = d_{31}\mathcal{E}_3 \tag{A1}$$

However, this mechanical/electrical coupling coefficient d_{31} has been found to be dependent on strain.[20] In addition,

piezoceramics were found to exhibit hysteresis and limited orthotropy.

Because of the hysteresis, the strain history of the piezoceramic must be known in order for piezoceramic actuator systems to produce repeatable deformations and to match measured deformations to theoretical predictions. This can be accomplished by first establishing the residual strain state on the field-strain hysteresis loop, and then applying positive field. For this purpose, a one-sided secant coupling coefficient d in either the longitudinal (d_{31}) or transverse (d_{32}) direction is defined as

$$d = \frac{\epsilon}{\mathcal{E}} = \frac{\epsilon_{\text{pos}} - \epsilon_o}{\mathcal{E}} \tag{A2}$$

based on the difference in strain at some applied field (ϵ_{pos}) and zero applied field (residual strain ϵ_o).

It has been found that the relationship between the piezoceramic actuation strain and the applied field also is altered by elastic constraints, because the mechanical/electrical coupling coefficient is dependent on the induced strain in the piezoceramic. The dependance of this coupling coefficient on induced strain necessitates the development of a relationship for predicting the actuation strains Λ created in constrained piezoceramics, which is

$$\Lambda = \begin{bmatrix} \Lambda_x \\ \Lambda_y \\ 0 \end{bmatrix} = \begin{bmatrix} d_{31}(\epsilon_x) \\ d_{32}(\epsilon_y) \\ 0 \end{bmatrix} \mathcal{E}_3 \tag{A3}$$

Functional relationships for the coupling coefficients $d(\epsilon)$ are found by fitting a curve through strain vs field data from unconstrained piezoceramics, as in Fig. A1. The induced strains, which are equal to the actuation strains for unconstrained actuators, can be represented in each orthogonal direction as

$$\Lambda = \epsilon = A\mathcal{E} + B\mathcal{E}^2 \tag{A4}$$

Solving for the coupling coefficient d yields the strain dependent expression

$$d(\epsilon) = \frac{A}{2} + \frac{A}{2}\sqrt{1 + \frac{4B\epsilon}{A^2}} \tag{A5}$$

Note the functional dependence of the coupling coefficient on the induced strain ϵ, and how the experimentally determined constants (A and B) from unconstrained actuators are used to predict the coupling coefficient. Expanding the term under the radical using a binomial expansion and substituting this result into Eq. (A3) yields

$$\begin{bmatrix} \Lambda_x \\ \Lambda_y \\ 0 \end{bmatrix} = \left\{ \begin{bmatrix} 1 \\ 1 \\ 0 \end{bmatrix} A + \begin{bmatrix} \epsilon_x \\ \epsilon_y \\ 0 \end{bmatrix} \frac{B}{A} \right\} \mathcal{E}_3 \tag{A6}$$

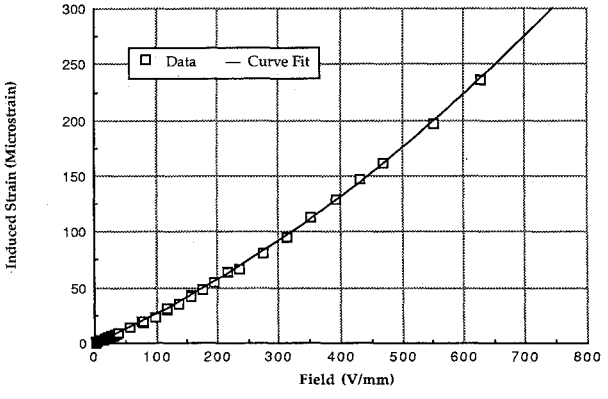

Fig. A1 Actuation strain vs applied field for an unconstrained piezoceramic. The experimental data and a curve fit, used in determining the mechanical/electrical coupling coefficient, are shown.

The actuation strain is dependent on the induced strain, since the actuation strain is directly proportional to the coupling coefficient. Thus, constraints on an actuator system that affect the coupling coefficient by altering the induced strain will also affect the actuation strain. Because of this dependence on induced strain and the use of experimentally determined constants, an iterative procedure was used to solve for the actuation and induced strains.

Acknowledgments

This research effort was supported by the General Dynamics Corporation with Michael Love and Jon Bohlmann serving as technical monitors.

References

[1]Jones, R. M., *Mechanics of Composite Materials,* Scripta, Washington, DC, 1975.

[2]Crawley, E. F., and de Luis, J., "Use of Piezoelectric Actuators as Elements of Intelligent Structures," *AIAA Journal,* Vol. 25, No. 10, 1987.

[3]Uchino, K., "Electrostrictive Actuators: Materials and Applications," *American Ceramic Society Bulletin,* Vol. 65, April 1986, pp. 647-652.

[4]Butler, J. L., *Application Manual for the Design of ETREMA Terfenol-D Magnetostrictive Transducers,* Edge Technologies, Inc., 1988.

[5]Shimuzu, K., Otsuka, K., and Shimizu, K., "Pseudoelasticity and Shape Memory Effects in Alloys," *International Metals Review,* Vol. 31, No. 3, 1986. pp. 93-114.

[6]Tsai, S. W. and Hahn, H. T., *Introduction to Composite Materials,* Technomic, Stamford, CT, 1980.

[7]Crawley, E. F., de Luis, J., Hagood, N. W., and Anderson, E. H., "Development of Piezoelectric Technology for Applications in Control of Intelligent Structures," *Proceedings of the American Control Conference,* June 1988.

[8]Crawley, E. F., Warkentin, D. J., and Lazarus, K. B., "Feasibility Analysis of Piezoelectric Devices," Space Systems Lab., Massachusetts Inst. of Technology, Cambridge, MA, Rept. MIT-SSL #5-88, Jan. 1988.

[9]Lazarus, K. B., "Induced Strain Actuation of Isotropic and Anisotropic Plates," S. M. Thesis, Massachusetts Inst. of Technology, Cambridge, MA, 1989.

[10]Chiarappa, D. J., and Claysmith, C. R., "Deformable Mirror Surface Control Techniques," *Journal of Guidance and Control,* Vol. 4, No. 1, 1981.

[11]Atluri, S. N., and Amos, A. K., (eds.), *Large Space Structures: Dynamics and Control,* Springer Verlag, 1988.

[12]Forward, R. L., and Swigert, C. J., "Electronic Damping of Orthogonal Bending Modes in a Cylindrical Mast-Theory," *Journal of Spacecraft and Rockets,* Vol. 17, No. 1, 1981.

[13]Hanagud, S., Obal, M. W., and Meyyappa, M., "Electronic Damping Techniques and Active Vibration Control," AIAA Paper 85-0752, April 1985.

[14]Burke, S., and Hubbard, J. E., "Active Vibration Control of a Simply-Supported Beam Using a Spatially Distributed Actuator," *IEEE Control Systems Magazine,* Vol. 7, No. 6, 1987.

[15]Boriseiko, V. A., Grinchenko, V. T., and Ulitko, A. F., "Relations of Electroelasticity for Piezoceramic Shells of Revolution," translated from *Prikladnaya Mekhanika,* Vol. 12, No. 2, 1976.

[16]Antonyak, Y. T., and Vassergiser, M. E., "Calculation of the Characteristics of a Membrane-Type Flexural-Mode Piezoelectric Transducer," *Soviet Physics—Acoustics,* Vol. 28, 1980, pp. 294-302.

[17]Ashton, J. E., and Whitney, J. M., *Theory of Laminated Plates,* Technomic, Stamford, CT, 1970.

[18]Anderson, E. H., "Piezoceramic Induced Strain Actuation for One- and Two-Dimensional Structures," S. M. Thesis, Massachusetts Inst. of Technology, Cambridge, MA, 1989.

[19]Jensen, D. W., and Crawley, E. F., "Comparison of Frequency Determination Techniques for Cantilevered Plates with Bending-Torsion Coupling," *AIAA Journal,* Vol. 22, No. 3, 1984, p. 415.

[20]Aronov, B. S., "Effective Coefficients of Electromechanical Coupling in Piezoceramic Bodies," translated from *Prikladnaya Mekhanika,* Vol. 16, No. 10, 1980.